PERGAMON

International Journal of Solids and Structures 40 (2003) 4749–4768

INTERNATIONAL JOURNAL OF SOLIDS and STRUCTURES

www.elsevier.com/locate/ijsolstr

Experimental investigation of the stress–stretch behavior of EPDM rubber with loading rate effects

Ming Cheng, Weinong Chen *

Department of Aerospace and Mechanical Engineering, The University of Arizona, P.O. Box 210119 1130 N Mountain, Arizona, Tucson, AZ 85721-0119, USA

Received 1 December 2002; received in revised form 11 March 2003

Abstract

The tensile stress–stretch behavior of an ethylene–propylene–diene terpolymer (EPDM) was experimentally investigated, both in a quasi-static stretching rate range (<0.4/s) with a conventional material test machine and in a dynamic stretching rate range (2800/s–3200/s) with a split Hopkinson tension bar (SHTB) technique. Experimental data were then analyzed using the Ogden and Roxburgh's idealized Mullins effect modeling theory. Results show that the stress–stretch behavior is significantly dependent on stretching rate and the Mullins effect exists under dynamic loading. Furthermore, stretching rate only affects the material properties. The degree of damage in a stretched specimen is a function of only the maximum stretch ratio the specimen experienced.

Keywords: Rubber; Constitutive behavior; Mullins effect; Loading rate; Permanent set

1. Introduction

Cross-linked ethylene–propylene–diene terpolymer (EPDM) is one of the most commonly used industrial polymers because of its outstanding resistance to aging due to heat, light, oxygen, and ozone. The physical properties of EPDM and EPDM-based composites have been studied by many researchers (e.g., Zaharescu et al., 2000; Das et al., 2002), but few efforts have been focused on its constitutive behavior. Because EPDM has the potential to be used in blast/shock absorbing applications, it is necessary to model its constitutive behavior under both quasi-static and high loading-rate deformation conditions.

The constitutive behavior of an elastomeric material is not necessarily repeatable when it is loaded for the first few cycles (Bouasse and Carrière, 1903; Mullins, 1969). In order to accurately model the stress–strain response, one must record and understand the inelastic deformation history of the material over the initial loading cycles. The inelastic stress–strain behavior of elastomeric materials has been an area of active research for a long time. There have been numerous experimental and analytical studies addressing different

* Corresponding author. Tel.: +1-520-621-6114; fax: +1-520-621-8191.
E-mail address: weinong@u.arizona.edu (W. Chen).

0020-7683/03/$ - see front matter © 2003 Elsevier Ltd. All rights reserved.
doi:10.1016/S0020-7683(03)00182-3

characteristics of the elastomeric response, such as stress softening, hysteresis, permanent set, and loading-rate effect. For example, during the stress softening, phenomenon also known as Mullins effect (Mullins and Tobin, 1965; Harwood et al., 1965; Harwood and Payne, 1966a,b) is an elastomer undergoes significant softening during the first couple of loading cycles and then the material response approaches stability. The stress-softening phenomenon was first observed in simple uniaxial tension by Bouasse and Carrière (1903) on rubber vulcanizates, but Mullins (1947) distinguished himself by a thorough experimental study of carbon-black filled rubber vulcanizates, which has resulted in the effect bearing his name. The review article by Mullins (1969) refers to many early studies of this phenomenon in simple uniaxial extension. Interestingly, recent studies revealed that a similar effect exists in rubber's physical properties. For example, Sau et al. (1998) found that the conductivity of EPDM rubber composites changes significantly when subjected to mechanical stress and strain. It was found that there is a similarity in the change of modulus and electrical resistivity against degree of strain and frequency of strain for different samples.

In addition to the Mullins effect, nearly all engineering rubbers exhibit some degree of hysteresis and permanent set under cyclic loadings. For some filled rubber vulcanizates, hysteresis becomes insignificant once the Mullins effect is removed, i.e., after the first several loading cycles. The "permanent set" is a common terminology used in the rubber industry, and is often referred as residual strain in the literature. In this paper, we will refer to the conventional permanent set as the permanent strain set in order to distinguish it from another phenomenon (permanent stress set) that we will discuss later on.

The constitutive behavior of a rubber has been found to be strongly loading rate dependent. The effects of strain rate on stress-softening was probably first observed by Kraus et al. (1966) during their experiments on a carbon black-reinforced butadiene–styrene rubber. They reported that stress-softening depended on the product of the extension rate and a temperature function. Bergström and Boyce (2001) recently consummated a three-dimensional model that accounts for the rate dependence, but the Mullins effect was not considered. Analytical three-dimensional modeling of the Mullins effect has been the focus of recent research activities (Govindjee and Simo, 1991; Miehe, 1995; Beatty and Krishnaswamy, 2000; Ogden, 2001; DeSimone et al., 2001). Beatty and Krishnaswamy provided a theoretical foundation for modeling the Mullins effect in both incompressible and compressible isotropic materials (Beatty and Krishnaswamy, 2000; Krishnaswamy and Beatty, 2000). They considered the Mullins effect to be the result of internal stretch-induced damage and introduced a softening function to express the extent of the damage sustained by the material, which depends on the pre-experienced maximum strain state. A similar approach was taken in the model of the Mullins effect developed by Govindjee and Simo (1991). Using another approach, Ogden and Roxburgh (1999a) developed a phenomenological theory of pseudo-elasticity for the Mullins effect, in which they employed a softening variable controlled by the maximum energy state attained. The theory was modified by Ogden and Roxburgh (1999b) to enable the permanent strain set to be accommodated, although an explicit form of the model for such case is still under development (Ogden, personal communication, 2002). Despite of all of the research efforts on the Mullins effect, the effects of loading rate have not been considered.

The application of EPDM rubber in blast/shock environments inevitably requires an understanding of the loading-rate effects on the inelastic behavior of elastomeric materials. In this paper, the uniaxial tensile stress–strain behavior of EPDM rubber is experimentally investigated in the quasi-static strain rate range ($\dot{\varepsilon} = 0.004$–$0.4$/s) as well as in the strain rate range of a split Hopkinson tension bar (SHTB) ($\dot{\varepsilon} \approx 3000$/s). The experiments are designed in such a way that the strain rate and Mullins effect on the tensile stress–strain behavior can be studied based on the experimental results.

2. Grip design and strain evaluation

The EPDM characterized in this experimental research is manufactured by Gasket Specialties, Inc. (http://www.gasketspecialties.com/) according to the military standard (MIL-G-22050C). The quasi-static

experiments were performed using a hydraulically driven material testing system (MTS 810). This material testing system provides a ramp loading, with flexible adjustments to control cross-head rates. The stretching rate with this machine can reach up to approximately 0.5/s, for a 300%-elongation loading cycle on a specimen 6.5 mm in length and 7.5×1.6 mm^2 in cross-sectional area. For higher stretching rates in the dynamic range, a SHTB modified with pulse-shaping and single-pulse loading techniques is employed.

Due to the large stretch ratios achieved in the experiments and the high Poisson's ratio values for rubbery materials, attention must be paid to the details of how the specimen was clamped in order to obtain valid data. The grips also introduce minimum disturbances to the stress wave propagations in a SHTB when employed in dynamic tests. Here we describe the design of the grips used to firmly clamp the rubber specimen over the entire loading cycles and the strain evaluation made to verify that there was no slippage between the grip and the specimen.

Proper design of a tension test fixture is one of the obstacles in an experimental investigation of tensile properties of soft materials such as rubber. Because of the restrictions applied at the boundaries between the specimen and gripping surfaces, the stress state in the specimen is far from a simple uniaxial tension near the gripping area. The grip is typically designed as a metal clamp, which inevitably squeezes the rubber specimen into a thin sheet and reshapes the specimen inside and near the grip. Although less popular, there are a few alternative grips that were designed for clamping soft materials in an attempt to reduce the end effects. For example, a 'cryo-jaw' device (Riemersa and Schamhardt, 1982; Sharkey et al., 1995) was designed to introduce a coolant to cool the specimen section inside the jaw to a temperature below glass transition. Hardening of the soft specimen section by freezing can help the clamp to hold the specimen without significant reshaping. However, the temperature gradient on the specimen introduced by the freezing results in another form of inhomogeneous deformation near the grips, which complicates the stress–strain state. This inhomogeneity in specimen deformation becomes more serious if the material needs to be subjected to dynamic loading, where specimens must be short in order to achieve dynamic equilibrium. Besides clamping, another possible gripping method is to directly bond the specimen ends to smooth faces of the grips. For example, Miller (2001) attached the ends of cylindrical brain specimens to platens of a stress–strain testing machine using surgical glue. Since the glue provides restriction to the specimen, the specimen is not in a pure uniaxial tension state. Miller theoretically analyzed the strain state in the specimen and concluded that the deformed shape of a cylindrical specimen subjected to uniaxial extension is independent of the form of the constitutive law, and that the stretch at the symmetrical center is proportional to the distance between the ends of the specimen.

However, these alternative gripping designs are not applicable in the present research. The option of direct bonding the specimen to grips is not feasible due to the high tensile strength and poor compatibility of the EPDM material. The end-cooling option is not a possible gripping method due to the short specimen restrictions imposed by the dynamic test requirements in this research. Therefore, a metal clamp was designed that causes minimum disturbances to stress wave propagation in dynamic tensile experiments. The sections of the specimen inside the grips are squeezed to a thin and expanded sheet, as shown in Fig. 1, causing the stress state there and nearby to be non-uniaxial. However, this is the most feasible approach under the given restrictions of dynamic tensile testing on soft materials. The consequences of adopting this grip design is that the stress–strain behavior obtained from the experiments may not be exactly the behavior under uniaxial stress conditions. However, the results are still valid for the investigation of rate effects on the Mullins effect. Furthermore, the stretch measured from the grip separation may not be the specimen stretch under uniaxial stress condition. A calibration experiment was designed to relate the stretch measured by the displacement of the two grips to a one-dimensional specimen stretch based on Miller's (2001) analysis.

In this calibration experiment, the specimen is held at different stretch levels while the displacements between two grips are recorded to evaluate the strain applied on the specimen. The strain at the central portion of the specimen is measured by taking digital images of the previously marked central portion with

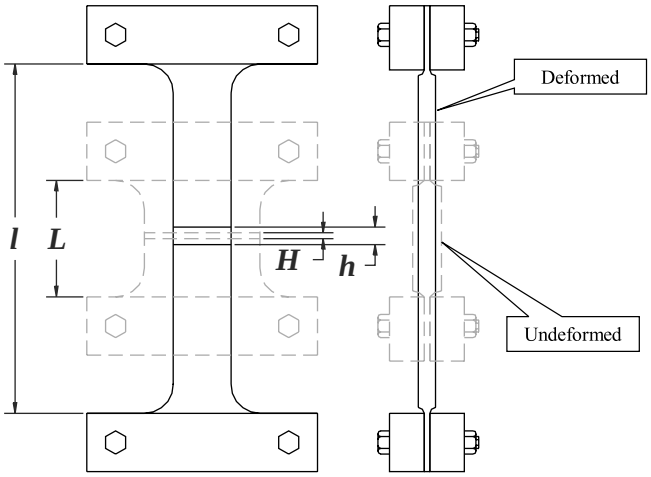

Fig. 1. A schematic description of deformed and undeformed configurations of the specimen.

grips because the dimensions of the specimen do not allow the use of a conventional extensometer to measure the strain at the central portion without the end effects from the grips. The calibration results of a specimen as shown in Fig. 1 are shown in Fig. 2, which indicate that the strain at the central portion of the specimen can be accurately evaluated by the displacement between grips with the same relationship Miller (2001) obtained for a cylindrical specimen,

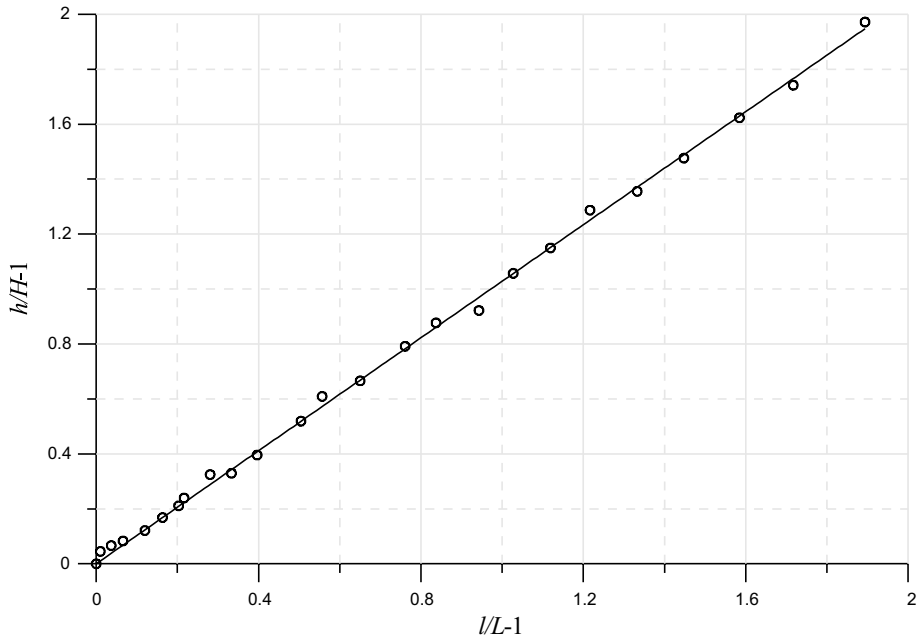

Fig. 2. Relationship between strains evaluated using the displacement between grips and those evaluated using direct measurement at the symmetrical central portion of the specimen.

$$\lambda - 1 = K\left(\frac{l}{L} - 1\right) \tag{1}$$

where λ is the stretch of specimen and the constant K is 1.0283 in this case of rectangular cross-section (7.5×1.6 mm^2) instead of 1.583 as in Miller's case of a circular cross-section. The fact that the value of K is less than 3% from unity indicates that the end effects in the specimen are not significant despite the employment of the direct clamping method. Several calibration experiments for the determination of K were conducted with specimen lengths (L) ranging 4–8 mm, which is the range covering the lengths of specimens used for this study. The fact that K remains a constant over the entire stretch range, as shown in Fig. 2, indicates that there cannot be measurable slippage between the specimen and the grips over the entire duration of the experiment. The cross-section of the calibration specimens was the same as that of the test specimens. The length range selected for this study is restricted by the requirement that dynamic force equilibrium must be maintained during dynamic loading for the purpose of measuring the material properties from the specimen under valid dynamic testing conditions. With confidence in the accuracy of the strain measurements as displayed in Fig. 2, tensile experiments were conducted on EPDM specimens under both quasi-static and dynamic loading conditions.

3. Quasi-static experiments

Quasi-static uniaxial tensile experiments were conducted at room temperature using a computer-controlled MTS servo-hydraulic testing machine operated in the displacement control mode. The EPDM specimens, with dimensions of 6.5 mm in length and 7.5×1.6 mm^2 in cross-sectional area, were subjected to loading cycles consisting of a set of constant strain-rate segments in order to probe strain-rate dependence during both loading and unloading. The strains were evaluated with cross-head displacements and corrected using Eq. (1) as discussed above.

3.1. Experimental results

In order to investigate the effects of loading rate and previous maximum stretch on the stress–strain response of the EPDM rubber, as well as the stress-softening behavior, a series of quasi-static tensile experiments was performed at various loading rates and stretch ratios. Experiments were also performed where loading rate and maximum stretch were systematically varied and repeated within one test to examine the inter-relationship between the loading rate and maximum stretch. The results of these experiments are summarized in Figs. 3–6. The stresses are reported as engineering stresses, which are loads per unit of original cross-sectional area. The abscissa used here is stretch, which is the current length of the specimen divided by the original length (l/L).

Fig. 3 shows the stress–stretch ratio curves obtained from a virgin specimen subjected the loading history shown as the insert in Fig. 3. The numbers in Fig. 3 indicate the loading cycle sequence. The loading was applied at a stretch ratio rate of 0.004/s. When the stretch ratio is less than 1.5, the top curve in the initial section ($0 < \lambda < 1.5$) of Fig. 3 is the first stress–stretch ratio curve obtained from the specimen when subjected to tensile loading. The curve exhibits a slightly non-linear behavior. At $\lambda = 1.5$, the testing machine was controlled to initiate unloading. As the cross-head moved backward, the stress in the specimen decreased. This unloading stress–stretch behavior is shown in Fig. 3 as the curve initiating at the first peak stress at $\lambda = 1.5$ and ending at zero stress but a small permanent stretch ($\lambda = 1.05$). This permanent stretch is called the permanent strain set. Since our calibration experiments showed there was no slippage between the specimen and the grips, the permanent stretch appearing in Fig. 3 is not from specimen slippage, but is the material behavior characterized as the permanent strain set. This is an indication that the

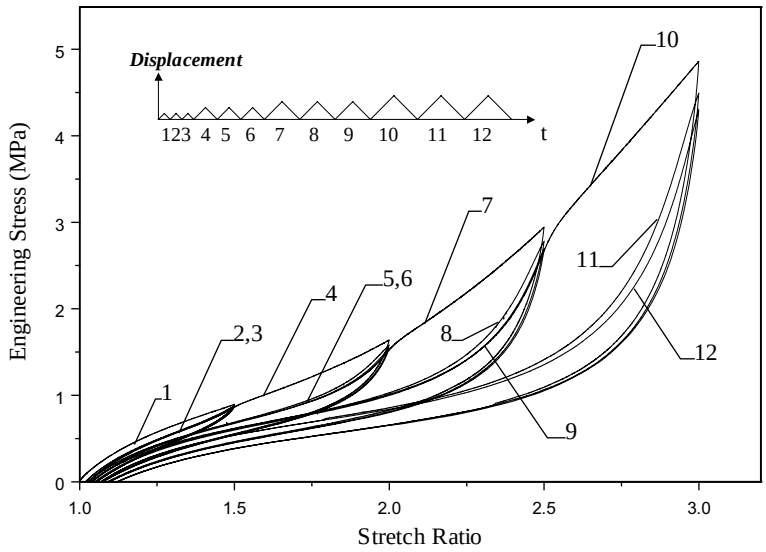

Fig. 3. Stress–stretch behaviors under loading rate 0.004/s.

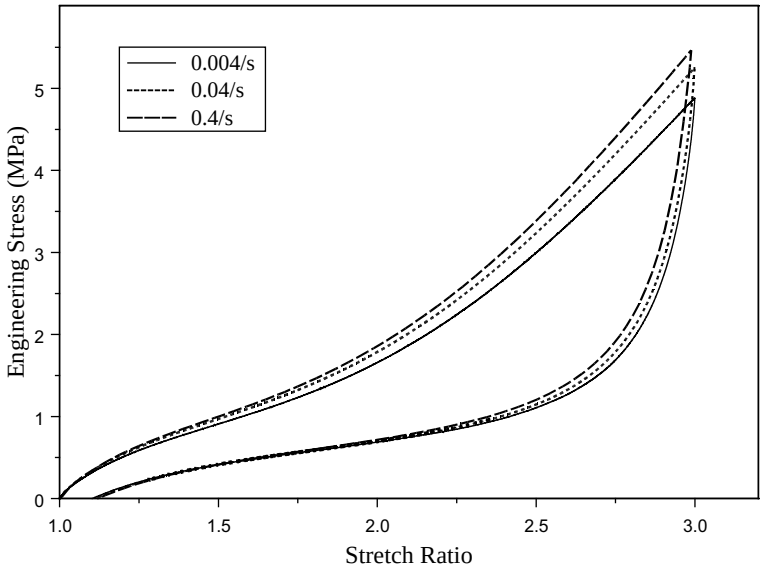

Fig. 4. Experimental results with different stretching rates.

microstructure of the specimen material has been permanently damaged by the loading cycle. It has been verified that the permanent strain set was not recoverable, even after leaving the specimen stress free (but clamped) for a week. The fact that the unloading curve is well below the loading curve indicates significant hysteresis over the loading cycle, another evidence of internal damage in the specimen caused by loading. After unloading, the specimen was reloaded back to a stretch ratio of $\lambda = 1.5$. The second loading curve has a similar trend as the first loading curve. However, the stress amplitude is well below that from the first

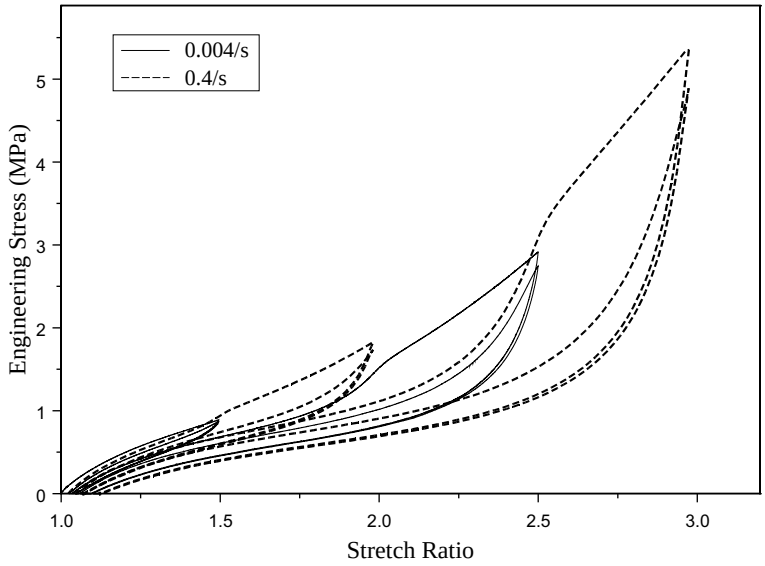

Fig. 5. Experimental results of a specimen with stretching rate sequence of 0.004/s–0.4/s–0.004/s–0.4/s.

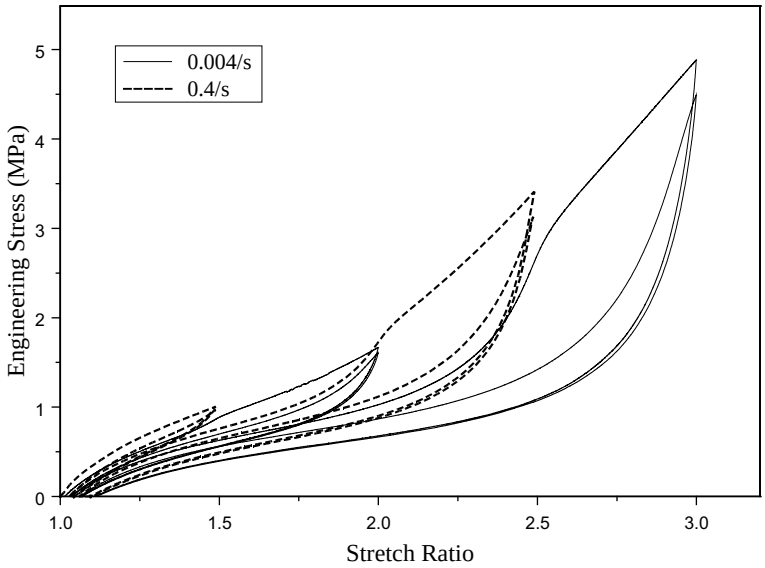

Fig. 6. Experimental results of a specimen with stretching rate sequence of 0.4/s–0.004/s–0.4/s–0.004/s.

loading curve at all stretches. This is a typical stress-softening phenomenon in elastomers, and is commonly known as the Mullins effect. When the specimen is stretched to $\lambda = 1.5$ for the second time, the stress achieved is slightly less than that achieved from the first time. We call this phenomenon, which has not been identified in the literature, permanent stress set.

At $\lambda = 1.5$, the specimen was unloaded again. The second unloading curve is similar to the first one except that the peak load is slightly lower and the permanent strain set is slightly larger when the stress

reaches zero. A third loading to $\lambda = 1.5$ resulted in very similar loading–unloading stress–stretch curves as those from the second loading cycle. This fact indicates that the internal damage in the specimen due to repeated loading is much less significant in the specimen if the maximum stretch from the first loading is not exceeded.

However, when the previous maximum stretch is exceeded, the loading–unloading behavior merges back to that from the first loading shortly after the previous maximum stretch. This is shown as the stress–stretch curve from loading cycle #4 in Fig. 3. When $\lambda < 1.5$, the loading stress–stretch curve nearly overlaps that from loading cycle #3. At $\lambda = 1.5$, the stress is slightly below that from loading cycle #1, by the amount of the permanent stress set. As the stretch ratio further increases from 1.5, the stress gradually increases to a level as if it was on the extension from the cycle #1 stress–stretch curve. The merge occurs at $\lambda \approx 1.6$. After $\lambda = 1.6$, the specimen deforms as if it was loaded for the first time. The specimen is eventually unloaded again at $\lambda = 2.0$. As the stretch decreases, significant hysteresis and the permanent strain set are again observed, as shown in Fig. 3. When the specimen is loaded by a 5th loading cycle to a maximum stretch ratio of 2.0, the Mullins effect and the permanent stress set are again observed, just as the observation from the second loading cycle except for the maximum stretch ratio. The same procedure is repeated again at maximum stretch ratios of 2.5 and 3.0, and similar stress–stretch behavior (hysteresis, Mullins effect, permanent strain set, and permanent stress set) is observed, as shown in Fig. 3, at different stretch levels.

The experimental results summarized in Fig. 3 demonstrate that substantial hysteresis occurs at any level of maximum stretch when the material is loaded to that maximum stretch for the first time. However, hysteresis decreases significantly over subsequent loading cycles at or below the previous maximum stretch level. This fact indicates that the maximum stretch in the loading history of an elastomer specimen dominates the amount of internal damage in the specimen from its virgin state. The results in Fig. 3 also show that both the permanent strain set and stress set increase with increasing maximum stretch, which means that the degree of permanent damage also depends on the stretch level applied on the specimen. An important phenomenon that repeats itself at all maximum stretch levels shown in Fig. 3 is the permanent stress set, the fact that the subsequent loading cannot reach the same stress level as the original loading at the maximum stretch. In order to reach the stress level, the stretch during the subsequent loading must exceed the maximum stretch on the original loading path. However, the subsequent loading merges into the original loading path, leaving a gap between the previous maximum stretch and the merging point. The stress in this gap is below the stress on the original loading path without unloading.

Significant stress softening, i.e., the Mullins effect, occurs at all maximum stretch levels between the first and second loading cycles. The subsequent loading causes further stress-softening on the specimen, but the degree of damage is much smaller than that from the original loading. We have conducted repeated experiments and found that it takes more than five repeated loading cycles for the EPDM specimen to reach its steady state, in which there is repeatability on the loading paths. However, the first loading cycle makes most of the contribution to the stress softening.

In order to investigate the loading rate effects on the stress–stretch behavior of the EPDM rubber, tensile experiments were performed at stretching rates of 0.004, 0.04, and 0.4/s. A virgin specimen was used for each experiment. The maximum stretch reached in these experiments was $\lambda = 3.0$. Fig. 4 shows the results from these experiments. The stress–stretch curve obtained from the first loading cycle at a stretching rate of 0.004/s shows behavior identical to the envelope of the stress–stretch curves loaded to a maximum stretch for the first time (i.e., the envelope of curves #1, 4, 7, and 10) in Fig. 3. As the loading rate increases, the stress levels at both the loading and unloading curves increase. At $\lambda = 3.0$, the stress increases from 4.88 MPa at $\dot{\lambda} = 0.004$/s to 5.46 MPa at $\dot{\lambda} = 0.4$/s. Therefore, the mechanical response of EPDM rubber is loading rate sensitive even within the quasi-static range.

In order to investigate the inter-relations among loading rate, maximum stretch, and stress softening, the loading rate and maximum stretch were varied and loading cycles were repeated within an experiment.

Figs. 5 and 6 show the results from such experiments. The results shown in Fig. 5 are for a virgin specimen that was stretched to a stretch of 1.5 at a stretching rate of 0.004/s. This loading was repeated three times to achieve a near steady state in the specimen (for clarity, only two cycles are shown in Fig. 5). The curves from the last two cycles are nearly overlapping. Then, the specimen was stretched to a stretch ratio of 2.0 for three repeated cycles at a stretching rate of 0.4/s. After these loading cycles, the specimen was further stretched to 2.5 for three repeated cycles with a stretching rate 0.004/s again, and finally, stretched to 3.0 for three repeated cycles at 0.4/s. On the other hand, a stretching rate sequence of 0.4/s, 0.004/s, 0.4/s, and 0.004/s was used for the experiments shown in Fig. 6. The stress–stretch curves in Figs. 5 and 6 show that the curves follow their monotonic behavior at various stretching rates, even though the stretching rate was switched back and forth in the middle of an experiment. Therefore, the results in Figs. 5 and 6 demonstrate that the effects of loading rate and maximum stretch on stress-softening are independent of each other, since inserting loading cycles with higher or lower loading rate does not change the behavior once the sequence reverts back to a loading path at the previous loading rate.

3.2. Phenomenological modeling

No unanimously accepted explanation of the mechanism of the Mullins effect in rubber materials is available so far. Mullins and Tobin (Mullins, 1969) proposed a quantitative and phenomenological stress-softening model, considering that the material is constituted by a soft phase and a hard phase. During deformation, hard regions are broken down and transformed into soft regions. Then the fraction of the soft region increases with increasing stretch. Mullins suggested that the stress softening is due to disentanglement of the network chains with the breakdown of interactions between the filler particles and the rubber matrix. Beatty and Krishnaswamy's (2000) model was based on this two-phase assumption of Mullins and Tobin, although their model does not cover loading-rate effect. They suggested that the hard phase of the model could be interpreted as clusters of molecular chains held together by short chain segments, chain entanglements, or inter-molecular forces.

Our results shown in Figs. 5 and 6 corroborate that, in the limited range of a low stretching rate (at least <0.4/s), the degree of damage is independent of the loading rate and the loading rate only affects the material parameters. Therefore, we divide the effects of loading-rate on the stress–stretch behavior of rubber materials into two parts. First, the material parameters used to describe the stress–strain behavior of rubber materials are dependent on loading rate, just as the well-known behavior of viscoelastic metals. Unlike in metals, the material damage in rubber materials occurs at the very beginning of stretch and continues as stretch increases. The second effect of loading rate on the stress–stretch behavior is degree of damage, which is usually described by most researchers as a scalar monotonically increasing function of maximum stretch experienced by the material.

Ogden and Roxburgh (1999a) developed a phenomenological theory of pseudo-elasticity to model an idealized Mullins effect under quasi-static loading, which considers the stress–stretch behavior without hysteresis and permanent sets. Later, they modified this theory to provide a modeling frame that can accommodate the permanent strain set (Ogden and Roxburgh, 1999b). An explicit formulation is not yet available (Ogden, personal communication, 2002), although a model incorporating the permanent strain set was published by Holzapfel et al. (1999), but it is not proper for the description of rubber behavior due to its inflexibility.

There are many other models for the description of the behavior of rubber under quasi-static loading. For example, Beatty and Krishnaswamy (2000) developed a theory of stress-softening in incompressible isotropic materials by introducing a stress-softening variable, which is a monotonically increasing function of the maximum previous strain experienced by the material. Marckmann et al. (2002) recently proposed a modified version of Arruda and Boyce's (1993) eight-chain model to accommodate the description of the Mullins effect. However, there is no model available that can accommodate all of the properties investigated

in this research, i.e., Mullins effect, permanent strain set, permanent stress set, hysteresis, and loading rate effects. In the following, Ogden and Roxburgh's (1999a) idealized Mullins effect modeling theory will be employed to describe the behavior of EPDM rubber under low loading rates ($\leqslant 0.4$/s) heuristically. Although this model does not cover permanent sets and loading rate effects, it does provides much flexibility, allowing it to give a better description of the stress–stretch behavior of rubber materials.

The stress–stretch behavior on the original loading path was described by Ogden and Roxburgh (1999a) using a strain-energy function in the usual way for an incompressible hyperelastic material as follows,

$$\sigma_1 - \sigma_3 = \lambda_1 \frac{\partial W}{\partial \lambda_1}, \quad \sigma_2 - \sigma_3 = \lambda_2 \frac{\partial W}{\partial \lambda_2} \tag{2}$$

where σ_i ($i = 1$, 2 and 3) are the principal Cauchy stresses, λ_i ($i = 1$, 2 and 3) are principal stretches, and W is a strain-energy function. Since incompressibility requires $\lambda_1\lambda_2\lambda_3 = 1$, the strain-energy function, W, is a function of λ_1 and λ_2 only. W is also taken to be a function of η, an additional variable that describes the internal damage state in the material and takes the value of unity on the original loading path, with the form as

$$W(\lambda_1, \lambda_1, \eta) = \eta \widetilde{W}(\lambda_1, \lambda_1) + \phi(\eta) \tag{3}$$

where ϕ is a smooth damage function subjected to $\phi(1) = 0$, $\widetilde{W}(\lambda_1, \lambda_1)$ is a strain-energy function characterizing the original loading path in (λ_1, λ_2)-space, which takes any standard form of the strain-energy function, such as the neo-Hookean or Ogden forms, and η is unity on the original loading path. On any unloading or subsequent submaximal loading, η is less than unity. Therefore, the Cauchy stresses are now given by

$$\sigma_1 - \sigma_3 = \eta\lambda_1 \frac{\partial \widetilde{W}}{\partial \lambda_1}, \quad \sigma_2 - \sigma_3 = \eta\lambda_2 \frac{\partial \widetilde{W}}{\partial \lambda_2} \tag{4}$$

Ogden and Roxburgh (1999a) proposed a particular form for $\phi(\eta)$ by considering all the restricting conditions for a strain-energy function. With this particular damage function, the parameter η was derived as

$$\eta(\lambda_1, \lambda_2) = 1 - \frac{1}{r}\operatorname{erf}\left\{ \frac{1}{m}\left[\widetilde{W}(\lambda_{1,\max}, \lambda_{2,\max}) - \widetilde{W}(\lambda_1, \lambda_2) \right] \right\} \tag{5}$$

where $\lambda_{i,\max}$ ($i = 1$ and 2) are maximum principal stretches attained on the original loading path, m and r are two empirical material parameters, and $\operatorname{erf}(\cdot)$ is the error function.

For simple tension on an incompressible material, the Cauchy stresses and principal stretches are

$$\sigma_1 = \sigma, \quad \sigma_2 = \sigma_3 = 0$$

and

$$\lambda_1 = \lambda, \quad \lambda_2 = \lambda_3 = \lambda^{-1/2}$$

By taking the Ogden form of the strain-energy function,

$$\widetilde{W}(\lambda_1, \lambda_2) = \mu \sum_{i=1}^{3} \frac{\mu_i}{\alpha_i}(\lambda_1^{\alpha_i} + \lambda_2^{\alpha_i} + \lambda_3^{\alpha_i} - 3) \tag{6}$$

we obtain the following model for engineering stress under simple tension loading,

$$\sigma_{\mathrm{E}} = \frac{\sigma}{\lambda} = \eta\mu \sum_{i=1}^{3} \mu_i \left(\lambda^{\alpha_i - 1} - \lambda^{-(\alpha_i/2)-1} \right) \tag{7}$$

with

$$\eta(\lambda) = 1 - \frac{1}{r}\mathrm{erf}\left[\frac{\mu}{m} \sum_{i=1}^{3} \frac{\mu_i}{\alpha_i} \left(\lambda_{\max}^{\alpha_i} - \lambda^{\alpha_i} + 2\lambda_{\max}^{-(\alpha_i/2)} - 2\lambda^{-(\alpha_i/2)} \right) \right] \tag{8}$$

where α_i, μ_i ($i = 1$, 2, and 3) and μ are material constants such that $2G = \mu \sum_{i=1}^{3} \mu_i \alpha_i$, $\mu_i \alpha_i > 0$ with G as the shear modulus in the reference configuration, and $\lambda_{\max}$ is the maximum stretch attained on the original loading path. Since the parameter μ can be absorbed into μ_i ($i = 1$, 2, and 3), it can be set to be unity under quasi-static loading. Since Ogden and Roxburgh's (1999a) model does not accommodate hysteresis, we consider only the loading path hereafter. Fig. 7 shows the results of non-linear least squares curve-fitting of stress–stretch ratio data at a stretching rate of 0.004/s.

Ogden and Roxburgh's (1999a) model can precisely describe the original loading path. However, it is not accurate enough to predict the subsequent loading paths. This is because Ogden and Roxburgh's model ignores the effects of the permanent strain set and permanent stress set. The material constants identified by non-linear least-squares curve fitting of experimental data with 0.004/s stretching rate are listed in Table 1.

As revealed by the experimental results shown in Figs. 5 and 6, the effects of loading rate and maximum stretch on the stress–stretch behavior can be considered independent of each other. The mechanism for this phenomenon is considered to be that the damage in the material depends only on the maximum stretch. The loading-rate in the quasi-static range is not high enough to induce additional damage in the material. Therefore, there is no need to include a parameter in the constitutive model to describe the coupling effect of loading rate and maximum stretch. Only material parameters are dependent on loading rate. Furthermore, the results shown in Fig. 4 indicate that one can only change parameter μ to describe the stress–stretch behavior at different loading rates. Fig. 8 shows the results of the model prediction for the

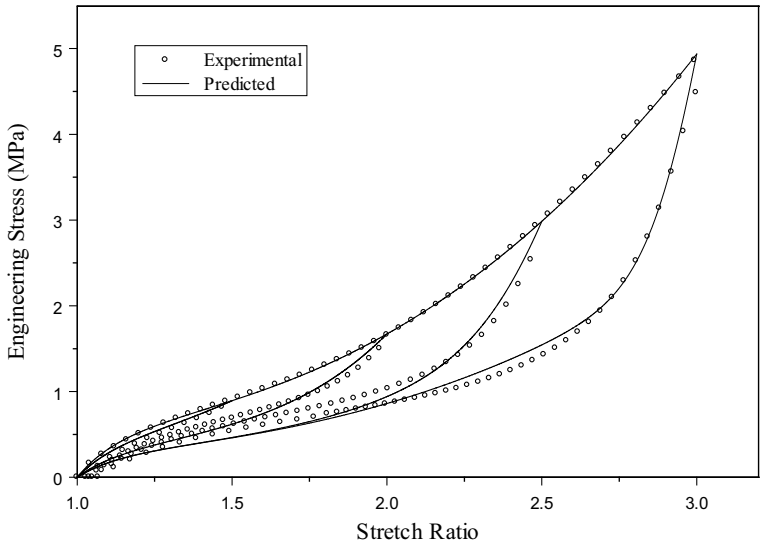

Fig. 7. Comparison between raw experimental data under loading rate 0.004/s and curve-fitting results with the Ogden and Roxburgh (1999a) model.

Table 1
Model parameters μ_i and α_i ($i = 1$, 2, and 3) at a stretching rate of 0.004/s

i	1	2	3
μ_i	744.9711	−239.0485	−0.3031
α_i	−0.0673	−0.2128	−7.2684
m		0.9773	
r		2.0620	

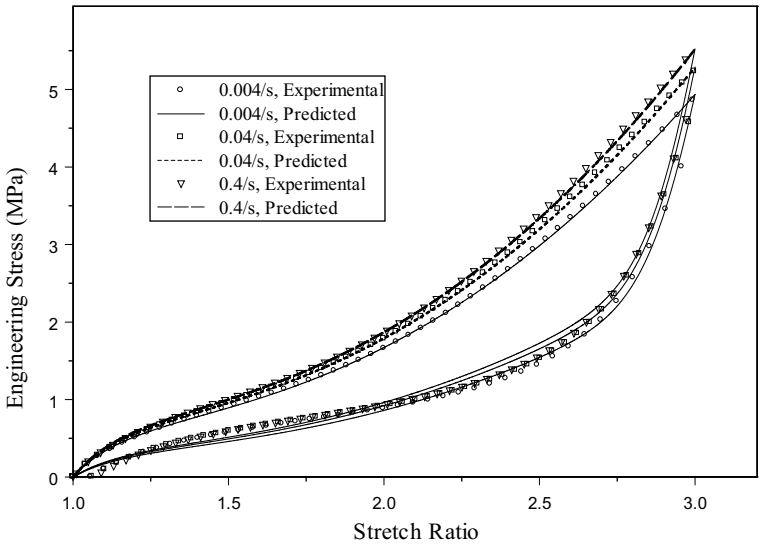

Fig. 8. Comparison between raw experimental data and predicted data with loading rate range under 0.4/s.

experiments shown in Fig. 4, which indicate that assuming only parameter μ as a function of loading rate is sufficient to give a description of the stress–stretch behavior of EPDM rubber. (The values of parameter μ at different loading-rates are listed in Table 2.) However, this conclusion is only justified by the experiments at stretching rates lower than 0.4/s. The proper loading-rate range needs to be identified by experiments at higher stretching rates, which is beyond the capacity of our quasi-static experimental facilities.

In order to determine if our conclusion that parameter μ as a function of loading rate in the quasi-static stretching rate range can be adapted to describe the stress–stretch behavior at varied stretching rates within the loading history of a specimen, the loading processes shown in Figs. 5 and 6 were predicted using Ogden and Roxburgh's (1999a) model (Eq. (7)) with parameters given in Tables 1 and 2. Figs. 9 and 10 are comparisons between predicted data and experimental data at mixing loading rates, and they further justify the conclusion that the variation of μ is sufficient to determine the rate effects in the quasi-static range investigated.

Table 2
Model parameter μ as a function of stretch rate

Stretching rate (/s)	0.004	0.04	0.4
μ	1	1.0713	1.1185

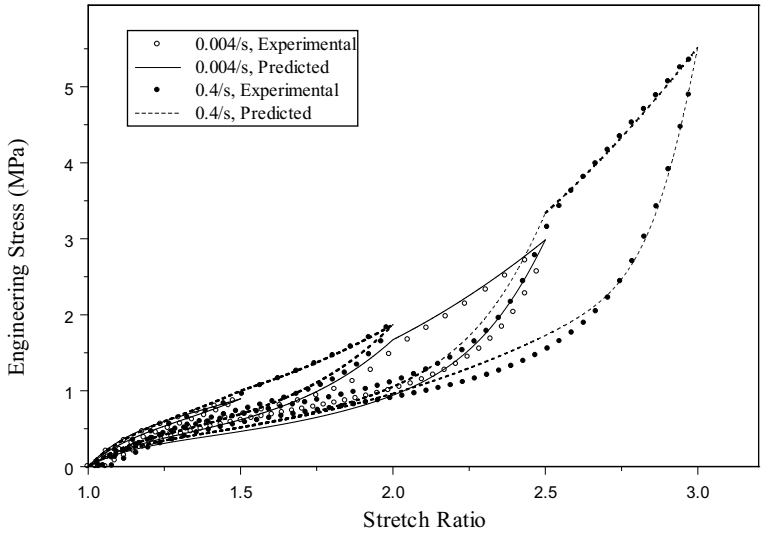

Fig. 9. Comparison between predicted data and experimental data with stretching rate sequence of 0.004/s–0.4/s–0.004/s–0.4/s.

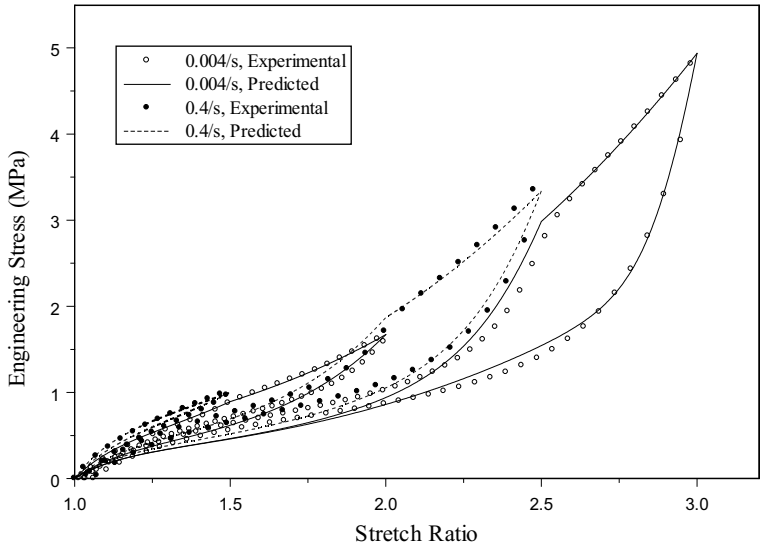

Fig. 10. Comparison between predicted data and experimental data with stretching rate sequence of 0.4/s–0.004/s–0.4/s–0.004/s.

4. Dynamic experiments

The SHTB experimental technique (Gray, 2000; Gray and Blumenthal, 2000) was employed to investigate the tensile stress–stretch behavior of the EPDM rubber under dynamic (high-rate) loading. When a soft specimen is tested with a SHTB, there is a dramatic mechanical impedance mismatch between the specimen and the bars. Such an impedance mismatch causes two significant problems associated with the accurate determination of the stress and strain histories in the specimen under dynamic

deformation. When the impedance of the specimen is much lower than that of the incident bar, nearly all of the incident pulse is reflected back to the incident bar, making the profile of the reflected signal nearly irrelevant to the specimen. However, according to the split Hopkinson bar data-reduction scheme, the reflected signal is proportional to the strain rate in the specimen, which should depend on the specimen material and its response to mechanical loading. On the other side of the specimen, only a very small stress pulse is transmitted into the transmission bar due to the very small strength and mechanical impedance of the soft specimen. This makes it very difficult to accurately determine the transmitted signal, which is proportional to the stress history in the specimen according to Hopkinson bar theory based on one-dimensional wave propagation, using conventional strain gages mounted on the bar surface.

A laser displacement measurement device was used to accurately measure the actual strain history in the specimen. The device includes a laser diode, a line head, and a photo detector. The details and working principles of the laser device are given by Ramesh and Narasimhan (1996). The only differences are that the setup was turned 90° from Ramesh and Narasimhan's design and an opening gap was measured instead of an expanding rod cross-section. A hollow bar technique (Chen et al., 1999) was used to accurately measure the transmitted force signal for stress assessment. To shorten the force disequilibrium period at the very beginning stage of the loading cycle and obtain a constant loading rate, a pulse-shaping technique (Chen et al., 2002) was employed. Furthermore, a momentum trapping technique (Nemat-Naser et al., 1991) was adopted to avoid undesired repeated loading on the specimen. A schematic illustration of the dynamic experimental setup is provided in Fig. 11.

During an experiment using the setup shown in Fig. 11, the gas gun speeds up a striker tube toward the flange. Once the striker tube impacts the flange, a tensile stress pulse is created within the incident bar and the end face of the flange moves toward the momentum trap bar. The momentum trap bar is initially placed a distance, δ, away from the flange, as shown in Fig. 11. The gap distance (δ) is set according to the particle velocity at the flange face during the tensile pulse period, such that the incident bar and the momentum trap bar are in full contact through the flange at the end of the loading pulse. Then, the tensile pulse travels

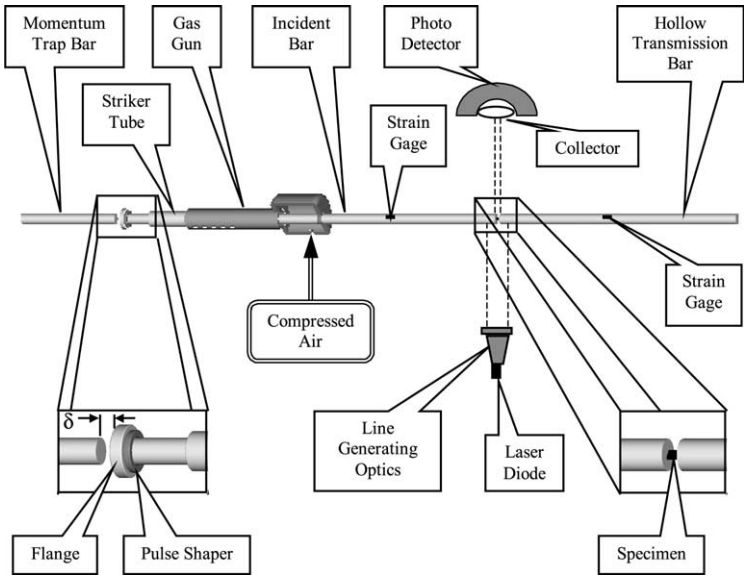

Fig. 11. Split Hopkinson tension bar with pulse shaping, momentum trap bar, hollow transmission bar and laser stretch measurement techniques.

toward the specimen, where it is partly transmitted into the transmission bar through the specimen and the rest of the pulse reflected as compression back into the incident bar. Since rubber materials are small in mechanical impedance compared with metal incident bars, the reflected compression is often nearly the same as the incident pulse. The reflected compression pulse is then transmitted into the momentum trap bar through the now-in-contact interface between the flange and momentum trap bar. The compression pulse crossing through the interface will be trapped in the momentum trap bar since the contact interface cannot support tension. In the experimental procedure, the gap setting is critical. Although this gap can be calculated by considering the gas gun's breech pressure, it provides a starting point that must be fine tuned in practice. This momentum trap bar technique was first proposed by Nemat-Naser et al. (1991). If this technique is not applied, the repeated tensile loading will overlap an extra specimen stretch on previous stretches, making it impossible to determine the maximum stretch the specimen experiences during one experiment, which is critical for examining the Mullins effect under high loading rates. The effects of the momentum trap bar are shown in Fig. 12.

Fig. 12(a) shows typical signals recorded in a dynamic SHTB experiment. With the successful application of the momentum trap bar technique, only one tensile pulse was applied on the specimen. In this case, the maximum stretch can be determined from the stretch record since the stretch decreases after the first tensile pulse. If the gap (δ) is not set properly, multiple tensile pulses will be applied on the specimen, consecutively. For example, Fig. 12(b) shows the results when the gap (δ) is too big to activate the momentum trap bar. In this case, many tensile pulses can be recognized from the incident signal. Furthermore, the following repeated pulses still possess significant amplitudes that can further load the specimen. From the stretch signal in Fig. 12(b), we can see that the stretch goes up step by step upon the arrival of each tensile loading pulse. (The stretch reaches a very high level that is beyond the scope of our recording instrument.) Meanwhile, the strain signal in the transmission bar is amplified more and more because of the repeated loading. Both the stretch and transmitted signals in Fig. 12(b) are clipped since the input range of our recording instrument is ± 10 V.

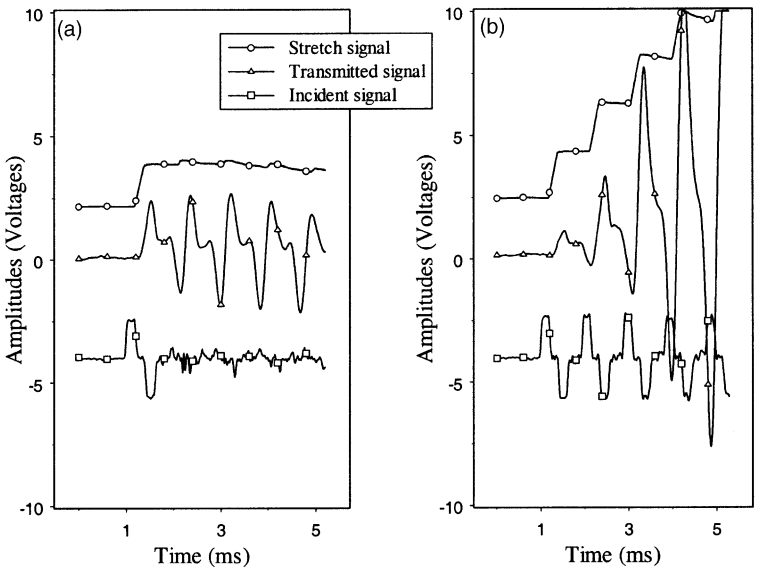

Fig. 12. Typical signals recorded in a dynamic experiment: (a) with momentum trap bar technique; (b) without momentum trap bar technique.

4.1. Experimental results

Fig. 13 shows the dynamic stress–stretch curves obtained from the dynamic SHTB experiments with the quasi-static experimental result at the stretching rate of 0.4/s embedded as a reference for the effects of loading rates. Due to the drastic mechanical impedance mismatch between the rubber specimen and the metal bars, the dynamic unloading behavior of the rubber specimen cannot be accurately recorded. Therefore, only the loading and early unloading portions of the dynamic stress–stretch curves are shown in Fig. 13. This drawback thwarts the plan to investigate the permanent strain set at high stretching rate using the SHTB technique. The results displayed in Fig. 13 reveal that the EPDM rubber possesses a significant rate-dependent constitutive behavior in tension. The stress reaches much higher values at the stretching rate of 3000/s than that at 0.4/s at the same stretch level. However, within a limited stretching rate range, for example, from 2800/s to 3000/s, it is difficult to tell any difference between their stress–stretch loading curves, as shown in Fig. 13.

In order to examine the stress-softening behavior (Mullins effect) at high stretching rates, three experiments were conducted sequentially on a specimen with short, middle, and long striker tubes. Since the length of the striker tube is proportional to the maximum stretch of the specimen provided the striker velocities at the moment of impact are kept the same, the maximum stretch with the second experiment is larger than the first, and the third is larger than the second. In this way, it is possible to obtain a series of loading curves with increasing maximum stretches. One set of experimental results with such a series of curves are shown in Fig. 14, in which the subsequent loading paths are below the original loading path before the stretch exceeds the previous maximum stretch. Three loading curves are shown in this figure. The first one is the loading curve generated by a short striker tube with a maximum stretch ratio of 1.30. The next loading curve with a maximum stretch ratio of 1.55 was generated by a middle-length striker tube. Finally, a long striker tube was used to cause the same specimen to stretch to about 1.85. Once the stretch on a subsequent loading exceeds the previous maximum stretch, the stress–stretch curve comes back to the original loading path the same as the stress–stretch behaviors observed under quasi-static loading conditions. Again, the unloading portions of the dynamic stress–stretch curves are not included in Fig. 14 due to

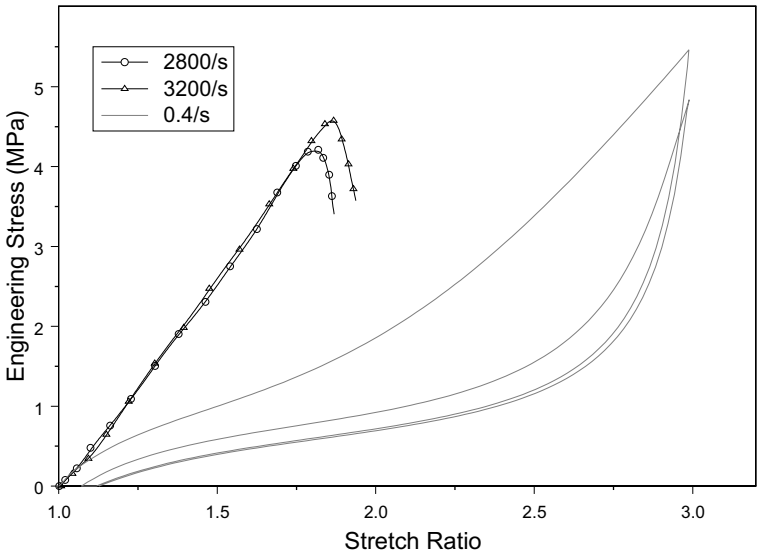

Fig. 13. Effects of high loading rates.

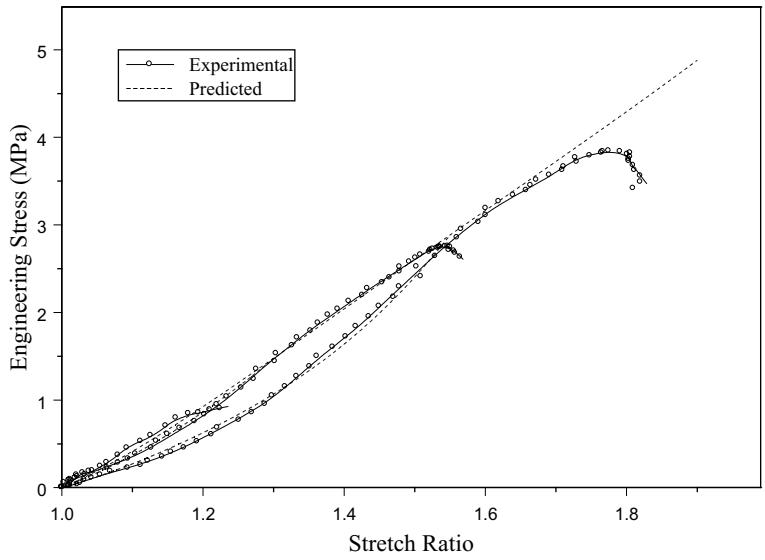

Fig. 14. Dynamic Mullins effect at a stretching rate of 3000/s.

poor accuracy. Furthermore, only one set of dynamic results is displayed for clarity of the presentation since all the SHTB results are very close, as shown in Fig. 13.

4.2. Phenomenological modeling

Heuristically, Ogden and Roxburgh's (1999a) model is employed again to explore the experimental results from dynamic tests. The model (Eq. (7)) is a phenomenological model; multiple sets of material parameters can be obtained by fitting into one stress–stretch curve. Therefore, a non-linear least-squares method was used to minimize the sum of the squares of the residuals between the experimental data and expected values. The material parameters obtained from the quasi-static experiments were used as starting estimates. Table 3 lists the curve-fitting results while the predicted behaviors with this set of material parameters are shown in Fig. 14.

In the quasi-static stretching rate range, it was found that the effects of stretching rate on the stress–stretch behavior of the EPDM rubber can be modeled as that part of material parameters are functions of the stretching rate. The model parameters associated with the degree of damage are independent of stretching rate. In dynamic case, it is interesting to note that the model parameters m and r, which are the

Table 3
Model parameters μ_i and α_i ($i = 1$, 2, and 3) at a stretching rate of 3,000/s

i	1	2	3
μ_i	188.6373	−1061.0986	−0.04922
α_i	−0.5281	−0.09549	−11.9074
m		0.9773	
r		2.0620	

indices of the degree of damage in Ogden and Roxburgh's (1999a) model, are the same in our dynamic experimental results as in the quasi-static experimental results.

5. Discussions

The stretching rate ranges covered in this experimental study of EPDM rubber were quasi-static (from 0.004/s to 0.4/s) and dynamic (from 2500/s to 3200/s). The upper bound of the quasi-static stretching rate range was limited by the capacity of the 810 MTS material testing machine while the lower bound of the dynamic stretching rate range was limited by the physical length of the SHTB. Even though there is a very large gap between the two loading rate ranges, the experimental studies in these two stretching ranges give a practical view of how the stretching rate affects the stress–stretch behavior of EPDM rubber. To obtain a comprehensive view of the stress–stretch behavior, the huge gap between these two stretching rate ranges must be filled. Therefore, new experimental techniques that can provide middle loading rates will have to be developed and employed.

In the phenomenological modeling of experimental results, Ogden and Roxburgh's (1999a) model was employed based on the assumption that the parameters in this model are rate-dependent. This assumption is justified by the phenomenological characteristic of this model. For a mechanism-based model, it is necessary to conduct more systematic dynamic experiments and examine the associated deformation/failure behavior to develop a fundamental understanding of the rubber deformation under high-rate loading including inertia effects.

6. Conclusions

Quasi-static and dynamic tensile experiments have been performed on an EPDM rubber. The grip design allows no slippage between the specimen and the grip over the entire duration of loading cycles, quasi-static or dynamic. The employment of a momentum trap bar and a short specimen in the SHTB technique ensured that the specimen was loaded by a single, well-defined, constant-rate loading history under dynamic equilibrium.

Besides the well-documented phenomena of the Mullins effect, hysteresis, and permanent strain set, the quasi-static experimental results revealed that a previously ignored behavior, named the permanent stress set, exists during cyclic loading. Both the permanent strain set and permanent stress set increase with increasing maximum stretch. Dynamic experimental results show that the Mullins effect also exists under high-rate loading. The rate effects are found to be associated only with the material properties. The damage state in the rubber varies only with the maximum stretch ratio.

Ogden and Roxburgh's (1999a) model was employed to describe the loading sections of the stress–stretch curves at various loading rates and maximum stretch ratios. This model can precisely predict the behavior of the quasi-static original loading path. However, it can only predict the subsequent loading path reasonably well, since it does not accommodate the effects of permanent strain set and permanent stress set.

The curve-fitted constants also show that the effects of stretching rate and maximum stretch on the stress–stretch behavior of EPDM rubber are independent of each other. For a low stretching rate such as 0.4/s and below, assuming only one parameter (μ) in the Ogden–Roxburgh model as a function of stretching rate is sufficient to give a good description of the stress–stretch behavior of EPDM rubber. However, this conclusion cannot be applied to the stress–stretch behavior of EPDM rubber at a high stretching rate such as 3000/s. Therefore, it is necessary to develop a new model to describe the stress–stretch behavior that includes the stretching rate effects on the material parameters. This new model

must also consider the effects of the permanent strain set and permanent stress set on the material properties.

Acknowledgements

This research was supported by Army Research Laboratory (ARL) through a grant (DAAD-19-00-1-0493) to The University of Arizona. The authors wish to thank Professor R.W. Ogden (Department of Mathematics, University of Glasgow, UK) for insightful email discussions.

References

Arruda, E.M., Boyce, M.C., 1993. A three-dimensional constitutive model for the large stretch behavior of rubber elastic materials. Journal of the Mechanics and Physics of Solids 41 (2), 389–412.

Beatty, M.F., Krishnaswamy, S., 2000. A theory of stress-softening in incompressible isotropic materials. Journal of the Mechanics and Physics of Solids 48, 1931–1965.

Bergström, J.S., Boyce, M.C., 2001. Constitutive modeling of the time-dependent and cyclic loading of elastomers and application to soft biological tissues. Mechanics of Materials 33, 523–530.

Bouasse, H., Carrière, Z., 1903. Courbes de traction du caoutchouc vulcanize. Annales de la Faculté des Sciences 5, 257–283.

Chen, W., Lu, F., Frew, D.J., Forrestal, M.J., 2002. Dynamic compression testing of soft materials. Journal of Applied Mechanics 69, 214–223.

Chen, W., Zhang, B., Forrestal, M.J., 1999. A split-Hopkinson bar technique for low impedance materials. Experimental Mechanics 39, 1–5.

Das, N.C., Chaki, T.K., Khastgir, D., 2002. Effect of processing parameters, applied pressure and temperature on the electrical resistivity of rubber-based conductive composites. Carbon 40 (6), 807–816.

DeSimone, A., Marigo, J., Teresi, L., 2001. A damage mechanics approach to stress softening and its application to rubber. European Journal of Mechanics—A/Solids 20, 873–892.

Govindjee, S., Simo, J.C., 1991. A micro-mechanically based continuum damage model for carbon black-filled rubber incorporating the Mullins effect. Journal of the Mechanics and Physics of Solids 39, 87–112.

Gray, G., 2000. Classic split-Hopkinson pressure bar testing. In: ASM Handbook, vol. 8. ASM International, pp. 462–476.

Gray, G., Blumenthal, W., 2000. Split-Hopkinson pressure bar testing of soft materials. In: ASM Handbook, vol. 8. ASM International, pp. 488–496.

Harwood, J.A.C., Mullins, L., Payne, A.R., 1965. Stress softening in natural rubber vulcanizates. Part II. Stress softening effects in pure gum and filler loaded rubbers. Journal of Applied Polymer Science 9, 3011–3021.

Harwood, J.A.C., Payne, A.R., 1966a. Stress softening in natural rubber vulcanizates. Part III. Carbon black-filled vulcanizates. Journal of Applied Polymer Science 10, 315–324.

Harwood, J.A.C., Payne, A.R., 1966b. Stress softening in natural rubber vulcanizates. Part IV. Unfilled vulcanizates. Journal of Applied Polymer Science 10, 1203–1211.

Holzapfel, G.A., Stadler, M., Ogden, R.W., 1999. Aspects of stress softening in filled rubbers incorporating residual strains. In: Dorfmann, A., Muhr, A. (Eds.), Constitutive Models for Rubber, pp. 189–193.

Kraus, G., Childers, C.W., Rollmann, K.W., 1966. Stress softening in carbon black-reinforced vulcanizates. Strain rate and temperature effects. Journal of Applied Polymer Science 10, 229–244.

Krishnaswamy, S., Beatty, M.F., 2000. The Mullins effect in compressible solids. International Journal of Engineering Science 38, 1397–1414.

Marckmann, G., Verron, E., Gornet, L., Chagnon, G., Charrier, P., Fort, P., 2002. A theory of network alteration for the Mullins effect. Journal of the Mechanical and Physics of Solids 50, 2011–2028.

Miehe, C., 1995. Discontinuous and continuous damage evolution in Ogden-type large-strain elastic materials. European Journal of Mechanics—A/Solids 14, 697–720.

Miller, K., 2001. How to test very soft biological tissues in extension. Journal of Biomechanics 34, 651–657.

Mullins, L., 1947. Effect of stretching on the properties of rubber. Journal of Rubber Research 16, 275–289.

Mullins, L., 1969. Softening of rubber by deformation. Rubber Chemistry and Technology 42, 339–362.

Mullins, L., Tobin, N.R., 1965. Stress softening in rubber vulcanizates. Part I. Use of a strain amplification factor to describe the elastic behavior of filler-reinforced vulcanized rubber. Journal of Applied Polymer Science 9, 2993–3009.

Nemat-Naser, S., Isaacs, J.B., Starrett, J.E., 1991. Hopkinson techniques for dynamic recovery experiments. Proceedings: Mathematical and Physical Sciences 435 (1894), 371–391.

Ogden, R.W., 2001. Pseudo-elasticity and stress softening. In: Fu, Y.B., Ogden, R.W. (Eds.), Nonlinear Elasticity—Theory and Applications. Cambridge University Press, pp. 491–522.

Ogden, R.W., Roxburgh, D.G., 1999a. A pseudo-elastic model for the Mullins effect in filled rubber. Proceedings of the Royal Society of London A 455, 2861–2877.

Ogden, R.W., Roxburgh, D.G., 1999b. An energy-based model for the Mullins effect. In: Dorfmann, A., Muhr, A. (Eds.), Constitutive Models for Rubber, pp. 23–28.

Ramesh, K.T., Narasimhan, S., 1996. Finite deformations and the dynamic measurement of radial strains in compression Kolsky bar experiments. International Journal of Solids and Structures 33 (25), 3723–3738.

Riemersa, D.J., Schamhardt, H.C., 1982. The cryo-jaw, a clamp designed for in vitro rheology studies of horse digital flexor tendons. Journal of Biomechanics 15, 619–620.

Sau, K.P., Chaki, T.K., Khastgir, D., 1998. The change in conductivity of a rubber-carbon black composite subjected to different modes of pre-strain. Composites Part A 29A, 363–370.

Sharkey, N.A., Smith, T.S., Lundmark, D.C., 1995. Freeze clamping musculo-tendinous junctions for in vitro simulation of joint mechanics. Journal of Biomechanics 28, 631–635.

Zaharescu, T., Meltzer, V., Vîlcu, R., 2000. Thermal properties of EPDM/NR blends. Polymer Degradation and Stability 70 (3), 341–345.